coatings

MDPI

Article

Improving the Laser Texture Strategy to Get Superhydrophobic Aluminum Alloy Surfaces

Annalisa Volpe [1,2,*], Sara Covella [1], Caterina Gaudiuso [1,2] and Antonio Ancona [1,2]

[1] Dipartimento Interateneo di Fisica, Università degli Studi di Bari, 70126 Bari, Italy; s.covella1@studenti.uniba.it (S.C.); caterina.gaudiuso@uniba.it (C.G.); antonio.ancona@uniba.it (A.A.)
[2] Institute for Photonics and Nanotechnologies, CNR IFN, Via Amendola 173, 70126 Bari, Italy
* Correspondence: annalisa.volpe@uniba.it

Abstract: Changing the wetting properties of surfaces is attracting great interest in many fields, in particular to achieve a surface with a superhydrophobic behavior. Laser machining is an emerging technique to functionalize materials with high precision and flexibility without any chemical treatment. However, when it is necessary to treat large area surfaces laser-based methods are still too slow to be exploited in industrial productions. In this work, we show that by improving the laser texture strategy it is possible to reduce the laser processing time to produce superhydrophobic aluminum alloy surfaces. Three different surface texture geometries were micromachined; namely, square, circular and triangular lattice grooves. We found that if the spacing between the grooves is narrow, i.e., when the percentage of the textured surface is high, the volume of air trapped inside the micromachined structures plays an important role in the wetting behavior. Meanwhile, when the groove spacing approaches the droplet dimensions, the texture geometry has a preponderant influence. Based on these findings an appropriate choice of the laser texture strategy allowed the fabrication of superhydrophobic aluminum alloy surfaces with a 10% reduction of processing time.

Keywords: femtosecond laser; laser texturing; wettability; superhydrophobicity; aluminum alloy; aerospace applications; optimization

Citation: Volpe, A.; Covella, S.; Gaudiuso, C.; Ancona, A. Improving the Laser Texture Strategy to Get Superhydrophobic Aluminum Alloy Surfaces. *Coatings* **2021**, *11*, 369. https://doi.org/10.3390/coatings11030369

Academic Editor: Chi Wai Chan

Received: 3 March 2021
Accepted: 22 March 2021
Published: 23 March 2021

1. Introduction

Modifying the wettability of surfaces plays an important role in many application fields from aerospace [1,2] to civil engineering and [3] microfluidics [4]. In particular, recreating the superhydrophobicity (SH), namely surfaces with a high water contact angle (>150°) and a low contact angle hysteresis or roll-off angle (<10°) [5], is attracting many researchers aiming to obtain surfaces with anti-bacterial [6], anti-icing [7,8] and self-cleaning properties [9], for example.

Modifying the surface morphology by short/ultrashort laser micromachining represents a highly flexible green process that is applicable to a wide range of materials from metals [10,11] to polymers [12,13]. In particular, direct laser writing (DLW) is a flexible and fast choice to reproduce the superhydrophobicity of the lotus leaf.

However, upscaling this technology to an industrial level to functionalize large area surfaces at reasonable costs and times still requires dedicated research efforts starting with the choice of the most appropriate and cost-effective laser source and beam steering system and, finally, defining the quickest and most efficient texturing strategy [14,15].

In DLW, several laser sources have been employed from nanosecond (ns) [16] to ultrashort laser pulses [17]. Though ns-lasers represent a lower cost solution, when thermal effects have to be avoided and it is requested to machine precise and reproducible micrometric structures, ultrafast lasers are usually preferred [18]. The recent availability on the market of ultrashort laser sources delivering hundreds of watts [19] has opened the possibility to significantly improve the machining throughput. However, the heat accumulation phenomena observed as soon as the average power exceeds tens of watts compromise the

peculiar ultrashort laser machining quality. Therefore, to exploit the full power currently available from commercial ultrafast laser sources, it is crucial to implement a specific beam engineering strategy to avoid the thermal effects [20]. In particular, it is necessary to scan the machined surfaces moving the beams at speeds of the order of several hundreds of meters per second that cannot be achieved with conventional (galvanometer) scan systems. Therefore, the development of alternative beam deflection methods is a current research challenge. Schille et al. [21] have proposed a high-throughput laser machining system consisting of a high-speed polygon mirror-based scan system in conjunction with a picosecond laser source supplying multi-hundred Watt average laser powers to the substrates.

In addition to the development of high-power ultrashort lasers and high-speed scanners, the improving of the texturing strategy represents a further approach to increase the process efficiency.

Several texture geometries have been proven to be able to produce superhydrophobic surfaces on metallic substrates without the need for any chemical post-treatment [22]. Among all, cross-hatching laser texturing has been exploited by several authors. Microcell structures of different sizes have been investigated by Cardoso et al. [23] on aluminum alloys. The ns-laser textured sample exhibited superhydrophobic behavior after just an aging process consisting of exposure to ambient air for some days. A one-step fabrication method of SH steel surfaces has also been demonstrated by Wang et al. [24]. A regular microgrid structure composed of micropillars was processed by the picosecond laser scanning of a sequence of lines intersecting themselves at 90° with a variable hatch distance. After exposure to ambient air for 24 h, the samples exhibited superhydrophobicity. A microgrid texture pattern was also produced by direct laser writing on AA2024 by Volpe et al. [25]. Here, the influence of the hatch distance between consecutive laser-scanned lines on the final wettability of the samples was investigated. After a thermal treatment that accelerated the aging process, superhydrophobicity was found for samples characterized by textures with a hatching distance below a certain threshold value.

A comparison between microgrid and other texture geometries has also been reported. Jagdheesh compared the wetting behavior of micropillars and microchannels [9] micromachined on aluminum by means of ns-laser pulses. Superhydrophobic and self-cleaning behaviors were reached after storing in ambient air for 24 h. A comparison between the wetting properties of an Al_2O_3 sample textured with microgrid and microholes was also reported in [26]. The two geometries were achieved by just changing the ps-laser parameters and maintaining the same crossed lines scanning pattern. A quite different geometry was investigated by the same authors for the fabrication in one step of near superhydrophobic aluminum surfaces by nanosecond laser ablation [27]. Two sets of blind microhole patterns produced with 40 and 80 pulses per microhole and with separation distance ranging from 15 to 35 μm were investigated. The samples processed with 80 pulses per microhole exhibited a better hydrophobicity with a water static contact angle value of $148° \pm 3°$. The superior wetting behavior was attributed to the higher depth of the blind microholes and to the height of the burrs of the recast melted material surrounding the microholes. These surface features were supposed to trap larger volumes of air that acted as a cushion to sustain the droplet resulting in a lower adhesion and superhydrophobicity [6,28–30]. Chen et al. [31] investigated three periodic surface patterns (triangle, circle and rhombus) to produce tunable superhydrophobic silicon surfaces by femtosecond laser (fs-laser) irradiation and a fluoroalkylsilane coating.

In the present study, we explore the possibility of reducing the laser processing time to obtain a superhydrophobic surface by changing the texture pattern. AA2024 was used as a substrate material due to the interest in changing its wetting properties in the aerospace and automotive industries. Three different texture geometries consisting of patterns of micrometric squares, triangles and circles with different densities per unit area were considered. For each texture, the volume of air trapped in the machined surface structures was estimated and correlated to the wetting behavior with the aim of identifying the best laser texturing strategy to produce superhydrophobic surfaces with less processing time.

2. Materials and Methods

Aluminum alloy sheets AA2024 with a dimension of 20 × 20 × 1 mm^3 and surface roughness (Ra) of about 200 nm cleaned in an ultrasonic bath with isopropyl alcohol were used for the experiments. The as-prepared samples were irradiated following the same setup previously reported in [25]. We employed a TruMicro Femto ed. Laser system (Trumpf GmbH, Ditzingen, Germany) emitting a linearly polarized beam at 1030 nm with a pulse duration of 900 fs. A two-mirror galvanometric scanner (IntelliSCAN 14, SCAN-LAB, Puchheim, Germany) equipped with a 100 mm telecentric lens was used to move and focus the beam over the sample following the desired texture path. The diameter of the Gaussian-profile beam at the focus was approximately 25 µm. The laser scanning parameters are reported in Table 1. All of the micromachining processes were carried out in ambient air.

Table 1. Laser and process parameters.

Wavelength	Pulse Duration	Pulse Energy	Scan Speed	Repetition Rate
1030 nm	900 fs	12.2 µJ	50 mm/s	50 Hz

After the irradiation, the samples were subjected to a heat treatment in a climate chamber (Temperature Test Chambers-ACS DY16T, Angelantoni Test Technologies Srl, Massa Martana (PG), Italy) at 100 °C for 24 h to accelerate the aging process.

The morphology of the samples was investigated through an Optical Microscope (Nikon Eclipse ME600, Nikon, Tokyo, Japan). The as-acquired images (Figure 1a) were analyzed by ImageJ (1.8.0, National Institutes of Health, Bethesda, MD, USA) [32] to determine the percentage of textured surface (%TS).

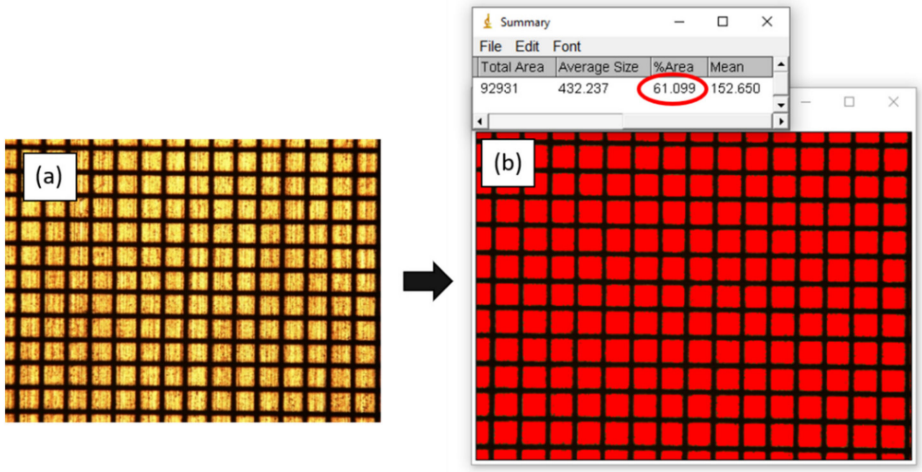

Figure 1. Example of image elaboration by ImageJ software. Here, a square lattice is reported (distance between consecutive scanning lines: h = 205 µm): (**a**) optical microscope view, (**b**) after processing with ImageJ. The percentage of the textured surface (dark lines) is 39%.

The threshold color function of ImageJ allowed the emphasis of the contrast between the laser ablated regions (Figure 1b, in black) and the untreated ones (Figure 1b, in red) and the function analyzed particles automatically calculated the percentage of the red untreated area (%Area). The percentage of the textured surface was thus obtained as %TS = 100 − %Area.

The surface wettability was evaluated by measuring the static contact angle (CA) of distillate water droplets by the sessile droplet method [5]. We used a digital goniometer, which consisted of a Dino-lite portable microscope and a cold light lamp for backlighting the droplet as reported in Figure 2.

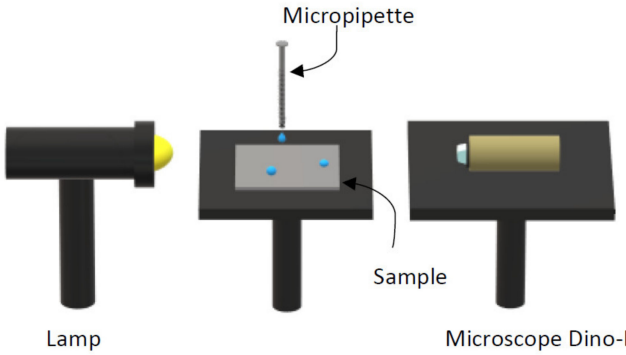

Figure 2. Schematic diagram of the contact angle measurement system.

Two different droplet volumes (2 and 10 µL) chosen in the measurable rainfall drop range size [33] were placed on the sample surfaces by means of a micropipette (see Figure 2). The measurements were performed at an ambient temperature of about 20 °C, placing three droplets of each volume in three different points of the machined area. The CA value of each water droplet was measured twice and the average value was calculated together with its standard deviation.

3. Results and Discussion

3.1. Fs-Laser Texturing of Aluminum Alloy Surfaces

Several regular microgrid texture patterns were created on the AA2024 samples by scanning the fs-laser beam over the surface. Each single laser track obtained processing samples with the parameters listed in Table 1 had a depth of 10 µm and a width of 25 µm. Three different textures were executed: square, triangular and hexagonal-circle lattices with a different microgrid spacing, *h*. Figure 3 shows the sketch of the three texture patterns in which the pitch *h*, the diameter *d* of the focal spot and the depth *l* of the laser ablated groove (black colored lines) are highlighted (Figure 3d).

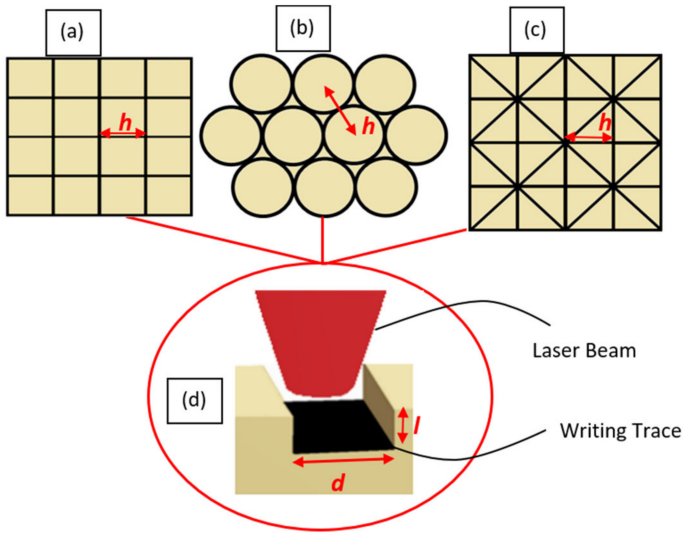

Figure 3. Sketch of the three different laser textured geometries: (**a**) square lattice; (**b**) hexagonal-circle lattice; (**c**) triangular lattice. The pitch *h*, the diameter of the focal spot *d* and the depth of the ablated groove *l* are highlighted in panel (**d**).

The square lattice was textured by scanning the surface in two perpendicular directions as shown in Figure 3a. The circle lattice was composed of rows of circles arranged in order to get the maximum packing, which was achieved by placing the centers of the circles

precisely at the vertices of a hexagonal lattice (Figure 3b). With this arrangement, the packing density (area of circles/total area) was equal to $\pi/(2\sqrt{3})$, corresponding to 90%.

The triangular lattice was obtained by scanning perpendicular lines (as well as for the square lattice) at a pitch distance h and then superimposing diagonal bisector lines as shown in Figure 3c.

Table 2 lists the samples produced and the corresponding pitch distance (h) and percentage of textured surface (TS).

Table 2. List of the fs-laser textured samples grouped based on the texture geometry. For each sample, the pitch distance (h) and the percentage of textured surface (TS) are reported.

Square			**Circle**			**Triangle**		
#	h (µm)	TS (%)	#	h (µm)	TS (%)	#	h (µm)	TS (%)
1	57	97	7	77	89	13	155	73
2	91	77	8	106	77	14	208	57
3	118	61	9	167	59	15	310	40
4	205	39	10	348	33	16	425	31
5	455	19	11	455	26	17	636	20
6	588	14	12	596	20	18	1272	13

It is worth noting that for each texture geometry there were some sections of the grooves where the laser beam passed two or more times. For instance, in the case of the square lattice there were four intersection points (highlighted in red in Figure 4a) in which the laser passed twice. Similarly, in the circle pattern there were six segments of the perimeter of each circle where the laser scanning path overlapped twice (highlighted in red in Figure 4b). Finally, for the triangular texture, two different types of overlaps occurred. As shown in Figure 4c, while in the red intersections the laser beam passed twice, in the green ones the laser path overlapped four times. Therefore, it was assumed that the ablated grooves were two times deeper in the red areas and four times deeper in the green ones compared with the rest of the texture.

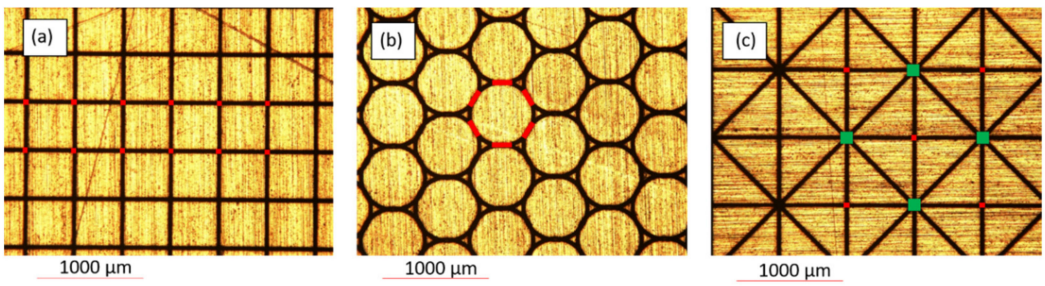

Figure 4. Microscopic images of the three textured geometries: (**a**) square lattice; (**b**) hexagonal-circle lattice; (**c**) triangular lattice. TS = 20%. In red and green are the overlapping areas of two and four laser lines, respectively.

Based on this assumption, the total ablated volume in a 1 mm × 1 mm portion of the textured area was estimated. It was further assumed that this quantity corresponded with the volume of trapped air per square millimeter of textured surface and it was plotted in Figure 5 as a function of the percentage of the textured surface. The points in the graph were grouped according to the pattern geometry.

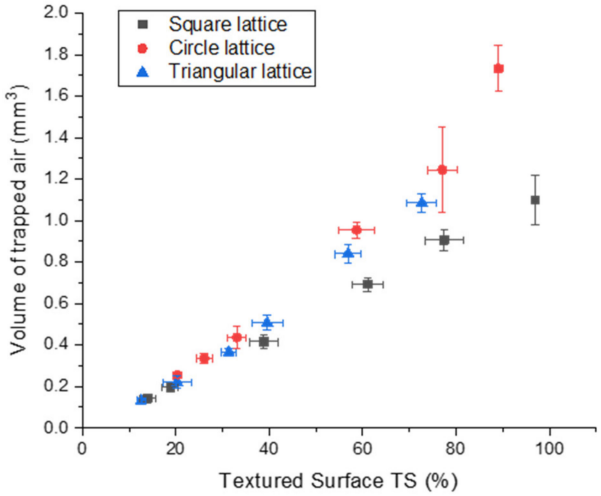

Figure 5. Volume of air trapped in a portion of 1 mm × 1 mm textured area as a function of the percentage of the textured surface (TS) for the three different texture geometries.

It can be noticed that for low percentages of TS, the ablated volume and thus the trapped air increased linearly and that, regardless of the geometry of the texture, almost all of the points on the plot resided on the same line. This happened because the density of the texture was still relatively low and the sections of the grooves where the ablation depth was different, depending on the texture geometry, were still very few to determine a substantial variation of the ablated volume per square millimeter. As the percentage of TS increased the texture geometry had a stronger influence on the total ablated volume, which was found to be higher for the circle lattice followed by the triangular lattice and then by the square texture.

3.2. Comparison between Fs-Laser Textured Geometries

The CA values registered for the untextured sample were 88° ± 1° and 83° ± 1° measured respectively with the 2 and 10 µL droplets. Thus, the hydrophilic nature of the aluminum alloy AA2024 surface was demonstrated as already reported in our previous study [25]. The difference between the two CA values can be related to the droplet weight, which, being greater in the 10 µL case, caused a wider spreading on the surface. The standard deviation of the CA measured values was always less than 1% thus demonstrating the repeatability of the measurements regardless of where the droplets were placed.

In Figure 6, the contact angle as a function of the percentage of the textured surface is reported for the droplet volumes 2 and 10 µL for the (a) square, (b) triangular and (c) circle lattice, respectively.

For all of the textures, a step trend of the CA was found. At a certain percentage of textured surface a sudden switch from hydrophobic to superhydrophobic behavior emerged, i.e., the water droplets did not adhere to the surfaces and, when released, bounced off. When this "fakir" condition occurs, it is conventionally established that the contact angle is equal to 180° [17,34]. Before this transition, a general increasing trend of the water CA with the percentage of TS (namely, when the hatch distance decreased) could be noted regardless of the volume of the droplets. The superhydrophobicity of the textured samples was attributed to the presence of the air trapped in the microstructures that acted as a cushion to hold up the water droplet [17]. The air cushions trapped in the laser textured structures impeded the effective contact with the water droplet. However, as the distance *h* increased, the fraction of hydrophilic aluminum surface in contact with the liquid increased causing a reduction of the contact angle. In addition to the role of the air trapped in the texture, the reduction of the CA could also be ascribed to the smaller percentage of TS as this portion of the surface underwent the chemical changes responsible for hydrophobicity. As reported by Van Den Brand et al. [35], hydrophobic properties are reached when

organic molecules, present in the ambient air moisture, attach to the micromachined surface. Organic molecules, being nonpolar, lower the total surface free energy. The X-ray photoelectron spectroscopy (XPS) analysis conducted by Cardoso et al. [23] on AA2024 samples observed a noticeable decrease of the carbon content after the laser texturing. This indicated that during the laser processing, organic molecules that were present in the original sample were removed by laser ablation. Conversely, after the aging, a higher concentration of carbon originated by the adsorption of molecules on the aluminum oxide layer formed after the laser treatment, was detected, which caused superhydrophobicity of the textured AA2024 surfaces.

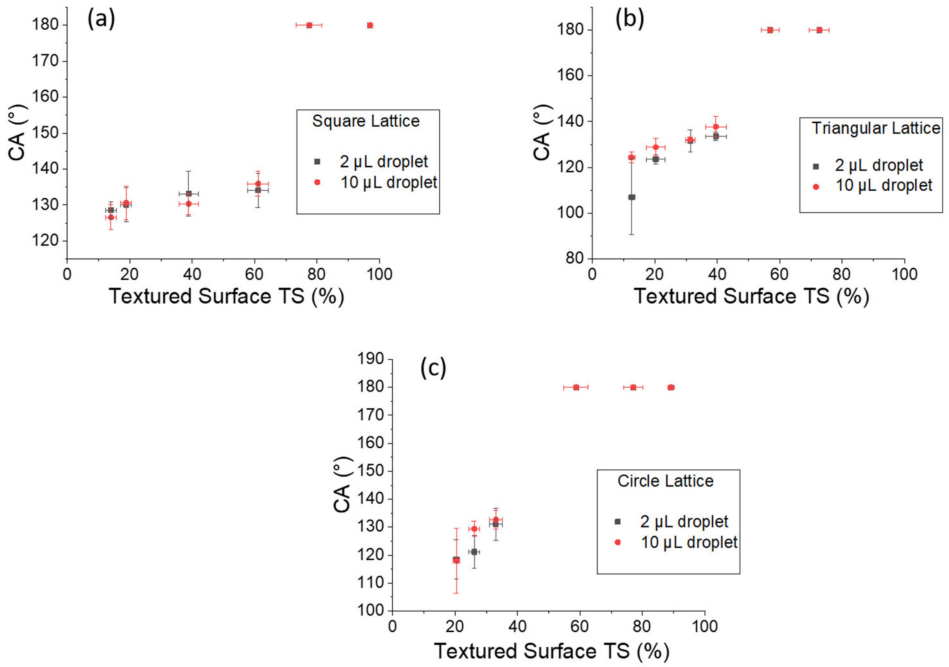

Figure 6. Evolution of the contact angle (CA) as a function of the textured surface percentage for 2 and 10 µL droplets: (**a**) square lattice, (**b**) triangle lattice, (**c**) circle lattice.

From Figure 6, it can also be noted that the droplet volume did not seem to influence the CA trend. The 10 µL droplets had a higher weight compared with the 2 µL ones, which should in principle cause an enlargement of the droplet and a lower CA. However, the bigger the droplets the larger the portion of the textured surface in contact with the droplet and thus the higher the sustaining force due to both air cushions and surface chemistry. This is believed to compensate for the higher gravitational force of the heavier droplet.

Further observing the results in Figure 6 it could be noticed that at lower percentages of TS the uncertainty associated with the CA measurement was greater. This could be related to the portion of the textured surface in contact with the droplets. Each droplet was, in fact, randomly deposited on the sample surface. As sketched in Figure 7, the contact area of the 2 µL droplet, whose diameter was around 1.7 mm, was comparable with the size of the grid. Therefore, we can suppose that a different positioning of the droplet resulted in a different enlargement and thus a quite different CA. Essentially, if the droplet was placed close to a laser ablation groove (Figure 7a), probably its spreading over the surface would be stopped at the groove location determining a higher CA. On the contrary, when the droplet was deposited far from the laser grooves (Figure 5b) a wider spreading was possible before reaching the closest ablation grooves thus resulting in a lower CA. Therefore, maintaining a texture pitch smaller than the droplet size allowed the production of surfaces with more reliable and reproducible wettability.

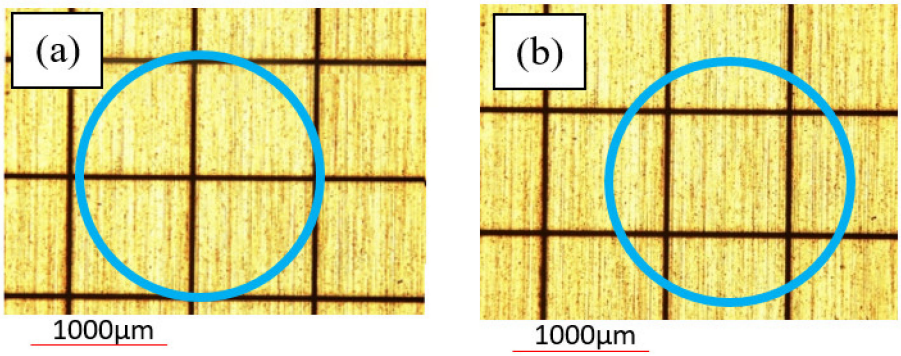

Figure 7. Sketch of two possible positions of a 2 µL droplet deposited on the square lattice having a pitch of 910 µm. The blue circle represents the droplet (**a**) enclosed by the crossed scan lines and (**b**) enclosing a machined square. The circle dimension was calculated for a droplet of 2 µL and a CA of 116° and resulted in being equal to 1.4 mm.

A direct comparison between the wetting behaviors of the three different geometries can be found in Figure 8 for the 2 µL droplets.

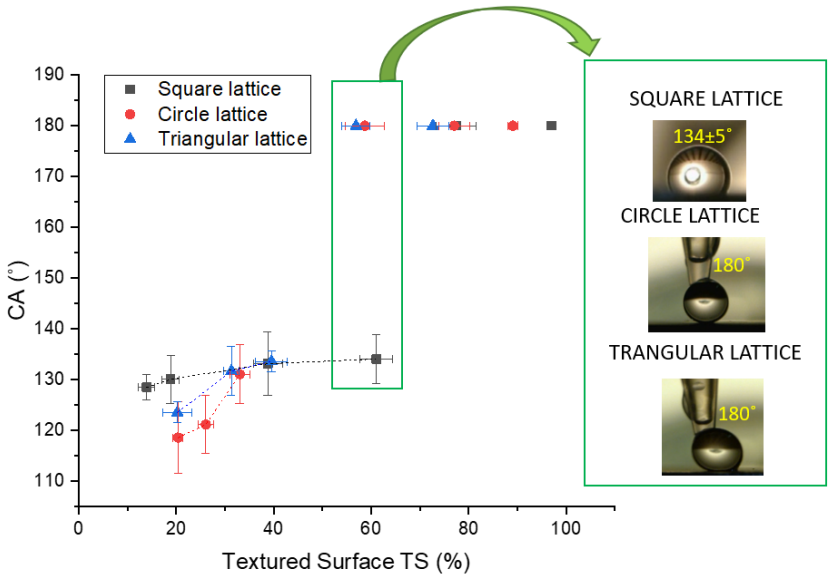

Figure 8. Evolution of the contact angle (CA) as a function of the percentage of the textured surface (TS) for the three different textures and a droplet volume of 2 µL. In the green rectangle, the images of the deposited droplet on the 60% textured samples are highlighted.

The rate of increase of the CA with the percentage of TS was different for the three textures. At a low TS, the square lattice showed the highest CA compared with the triangle and to the circle lattices. As the percentage of TS increased, the circle and triangle structures quickly reached the same hydrophobic properties of the square lattice and switched earlier to superhydrophobic behavior. The same results were observed for the 10 µL droplets as reported in Figure 9.

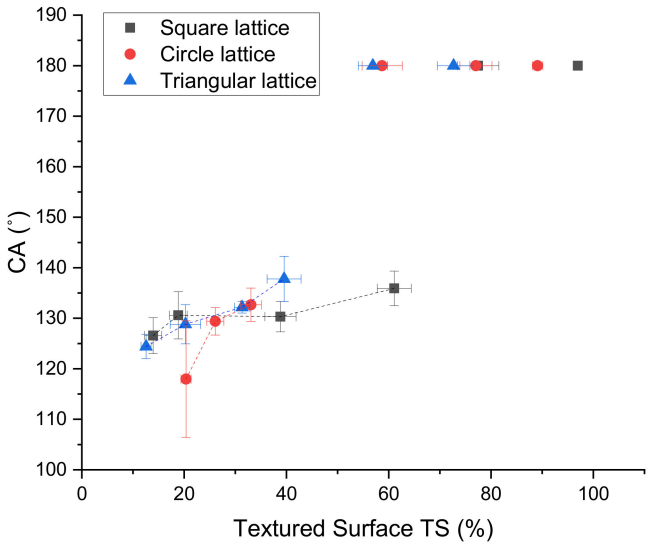

Figure 9. Evolution of the contact angle (CA) as a function of the percentage of the textured surface for the three different textures and a droplet volume of 10 µL.

The results represented in Figures 8 and 9 can be explained by taking into account the volume of air trapped by each texture geometry, which was estimated in Figure 5. Here, above a certain percentage of TS, the total ablated volume (namely, air trapped inside the microstructures) increased more rapidly for the circle and triangle geometries than the square texture. This justified the faster growth of the contact angle also observed in Figures 8 and 9. Samanta et al. [36] demonstrated how the degree of hydrophobicity depends on the amount of air entrapped in the textured surface. In their study, the durability of the superhydrophobic behavior of the surface was evaluated based on how long it maintained the air trapped in its pores, the so-called plastron. This is of critical importance in superhydrophobicity because it was shown that if the surface features were filled with water, the surface lost its water repellent properties and underwent a change from a Cassie–Baxter to a Wenzel wetting state [37]. It is worth noting that water can penetrate into the surface roughness through the vapor phase either by local condensation or by the application of high pressure or simply through droplet impact [38]. In the work of Li et al. [39] superhydrophobic surfaces were prepared characterized by hierarchical micro/nanostructures with interconnected micropores. The air plastron created by such surface features was shown to counteract external impalement hydraulic pressures up to 350 kPa. Similarly, in our case, the portion of the deeper textured sample could act as an air reserve. This air took the place of the air lost during the droplet impact improving the hydrophobicity of the sample. Therefore, the circle and triangle patterns ensured the transition to superhydrophobic behavior with a 20% less machined surface regardless of the size of the droplet. Consequently, the circle and triangle designs allowed a reduction of about 10% of the processing time to obtain SH, which means a significant saving of time and costs in large area surface texturing applications.

Conversely, for a low percentage of TS, the differences in the contact angle of the three geometries could no longer be correlated to the volume of trapped air and was comparable for all of the textures. The droplet dimension was of the same size as the hatch distance. However, the geometrical arrangement of the grooves forming the square lattice seemed to ensure a better confinement of the droplet compared with the other two textures. In the case of triangles and circles, with a similar percentage of TS, the separation between the ablated grooves was bigger thus causing a progressive widening of the drop and a lower value of the CA.

4. Conclusions

In this work, laser surface texturing technology based on ultrashort pulse laser ablation was used to modify the wettability properties of AA2024 aluminum alloy samples. Three different texture geometries consisting of groove lattices with square, triangular and circular patterns with a different percentage of textured surface, i.e., spacing between the grooves, were investigated. The purpose of the study was to identify which texture geometry ensured surface superhydrophobicity with the shortest laser processing time.

It was found that hydrophobicity strongly depends on the percentage of TS. For all of the texture geometries investigated the denser the lattice the higher the static CA of a droplet deposited on the surface. Above a certain percentage of TS there was a switch to superhydrophobicity where the water droplets did not adhere and bounced off the surfaces; thus, it was assumed that the CA was 180°. There were some differences depending on the texture geometry when this transition to superhydrophobicity occurred. For the triangle and circle patterns the threshold towards superhydrophobicity was observed at lower percentages of TS compared with square lattices. This behavior was explained taking into account that for a given percentage of textured surface, the circle and triangle patterns were characterized by a greater total ablated volume due to the fact that to produce those structures the laser scanning path overlapped more times in some parts generating deeper grooves at those intersections. Therefore, more air was trapped beneath the surface. Such air was supposed to act as a cushion and sustain the droplets, thus causing the SH behavior. We replicated the wetting experiments with two different droplet sizes and found the same results.

In conclusion, the circular and triangular geometries allowed us to obtain superhydrophobic surfaces with a lower percentage of machined substrate, thus saving about 10% of laser processing time compared with the square pattern with equivalent percentage of TS.

This result is very valuable and gives useful indications for the laser-based fabrication of large area superhydrophobic surfaces and the upscale of this technology to an industrial production level. Moreover, a similar strategy might be promising to texture other interesting materials such as stainless steel and Ti6Al4V. The latter is an alloy commonly used for aerospace components.

Author Contributions: Conceptualization, A.V.; experiments and data analysis A.V. and S.C.; writing—original draft preparation, A.V.; writing—review and editing, A.V., C.G. and A.A.; supervision and funding acquisition, A.A. All authors have read and agreed to the published version of the manuscript.

Funding: This research was funded by the Italian Ministry of Education, University and Research (MIUR) within the Project PON AIM184902B-1-ATT1 and by the Apulian Region within the "Research in Innovation" program (Project FEB1B50F) in the framework of POR PUGLIA FESR—FSE 2014/2020.

Institutional Review Board Statement: Not applicable.

Informed Consent Statement: Not applicable.

Data Availability Statement: Data is contained within the article or supplementary material.

Acknowledgments: The authors gratefully acknowledge Calabrese for his technical support Gianfranco Palumbo for providing us the materials and Francesco Giordano and Leonardo Di Venere for the climate chamber used in the experiments.

Conflicts of Interest: The authors declare no conflict of interest.

References

1. Liu, Z.; Zhang, F.; Chen, Y.; Zhang, H.; Han, Y.; Liu, J.; Huang, L.; Liu, X. Electrochemical fabrication of superhydrophobic passive films on aeronautic steel surface. *Colloids Surf. A Physicochem. Eng. Asp.* **2019**, *572*, 317–325. [CrossRef]
2. Ng, Y.H.; Tay, S.W.; Hong, L. Formation of icephobic surface with micron-scaled hydrophobic heterogeneity on polyurethane aerospace. *ACS Appl. Mater. Interfaces* **2018**, *10*, 37517–37528. [CrossRef]

3. Xiang, T.; Lv, Z.; Wei, F.; Liu, J.; Dong, W.; Li, C.; Zhao, Y.; Chen, D. Superhydrophobic civil engineering materials: A review from recent developments. *Coatings* **2019**, *9*, 753. [CrossRef]
4. De Marco, C.; Eaton, S.M.; Suriano, R.; Turri, S.; Levi, M.; Ramponi, R.; Cerullo, G.; Osellame, R. Surface properties of femtosecond laser ablated PMMA. *ACS Appl. Mater. Interfaces* **2010**, *2*, 2377–2384. [CrossRef]
5. Butt, H.J.; Roisman, I.V.; Brinkmann, M.; Papadopoulos, P.; Vollmer, D.; Semprebon, C. Characterization of super liquid-repellent surfaces. *Curr. Opin. Colloid Interface Sci.* **2014**, *19*, 343–354. [CrossRef]
6. Mateescu, M.; Knopf, S.; Mermet, F.; Lavalle, P.; Vonna, L. Role of trapped air in the attachment of staphylococcus aureus on superhydrophobic silicone elastomer surfaces textured by a femtosecond laser. *Langmuir* **2020**, *36*, 1103–1112. [CrossRef]
7. Wang, Y.; Xue, J.; Wang, Q.; Chen, Q.; Ding, J. Verification of icephobic/anti-icing properties of a superhydrophobic surface. *Appl. Mater. Interfaces* **2013**, *5*, 3370–3381. [CrossRef] [PubMed]
8. Volpe, A.; Gaudiuso, C.; Ancona, A. Laser fabrication of anti-icing surfaces: A review. *Materials* **2020**, *13*, 5692. [CrossRef]
9. Jagdheesh, R.; Diaz, M.; Oca, J.L. Bio inspired self-cleaning ultrahydrophobic aluminium surface by laser processing. *RSC Adv.* **2016**, *6*, 72933–72941. [CrossRef]
10. Ancona, A.; Joshi, G.S.; Volpe, A.; Scaraggi, M.; Lugarà, P.M.; Carbone, G. Non-uniform laser surface texturing of an un-tapered square pad for tribological applications. *Lubricants* **2017**, *5*, 41. [CrossRef]
11. Trotta, G.; Vázquez, R.M.; Volpe, A.; Modica, F.; Ancona, A.; Fassi, I.; Osellame, R. Disposable optical stretcher fabricated by microinjection moulding. *Micromachines* **2018**, *9*, 388. [CrossRef] [PubMed]
12. Volpe, A.; Paiè, P.; Ancona, A.; Osellame, R. Polymeric fully inertial lab-on-a-chip with enhanced-throughput sorting capabilities. *Microfluid. Nanofluid.* **2019**, *23*, 37. [CrossRef]
13. Volpe, A.; Trotta, G.; Krishnan, U.; Ancona, A. Prediction model of the depth of the femtosecond laser micro-milling of PMMA. *Opt. Laser Technol.* **2019**, *120*, 105713. [CrossRef]
14. Putignano, C.; Scarati, D.; Gaudiuso, C.; Di Mundo, R.; Ancona, A.; Carbone, G. Soft matter laser micro-texturing for friction reduction: An experimental investigation. *Tribol. Int.* **2019**, *136*, 82–86. [CrossRef]
15. Fraggelakis, F.; Giannuzzi, G.; Gaudiuso, C.; Manek-Hönninger, I.; Mincuzzi, G.; Ancona, A.; Kling, R. Double- and multi-femtosecond pulses produced by birefringent crystals for the generation of 2D laser-induced structures on a stainless steel surface. *Materials* **2019**, *12*, 1257. [CrossRef]
16. Samanta, A.; Wang, Q.; Shaw, S.K.; Ding, H. Nanostructuring of laser textured surface to achieve superhydrophobicity on engineering metal surface. *J. Laser Appl.* **2019**, *31*, 022515. [CrossRef]
17. Zhang, D.; Chen, F.; Yang, Q.; Yong, J.; Bian, H.; Ou, Y.; Si, J.; Meng, X.; Hou, X. A simple way to achieve pattern-dependent tunable adhesion in superhydrophobic surfaces by a femtosecond laser. *ACS Appl. Mater. Interfaces* **2012**, *4*, 4905–4912. [CrossRef] [PubMed]
18. Ancona, A.; Carbone, G.; De Filippis, M.; Volpe, A.; Lugarà, P.M. Femtosecond laser full and partial texturing of steel surfaces to reduce friction in lubricated contact. *Adv. Opt. Technol.* **2014**, *3*, 539–547. [CrossRef]
19. Du, K.; Brüning, S.; Gillner, A. High-power picosecond laser with 400 W average power for large scale applications. *Laser-Based Micro Nanopackag. Assem. VI* **2012**, *8244*, 82440P.
20. Mincuzzi, G.; Rebière, A.; Faucon, M.; Sikora, A.; Kling, R. Beam engineering strategies for high throughput, precise, micro-cutting by 100 W, femtosecond lasers. *J. Laser Appl.* **2020**, *32*, 042003. [CrossRef]
21. Schille, J.; Schneider, L.; Streek, A.; Kloetzer, S.; Loeschner, U. High-throughput machining using a high-average power ultrashort pulse laser and high-speed polygon scanner. *Opt. Eng.* **2016**, *55*, 096109. [CrossRef]
22. Wang, X.C.; Wang, B.; Xie, H.; Zheng, H.Y.; Lam, Y.C. Picosecond laser micro/nano surface texturing of nickel for superhydrophobicity. *J. Phys. D Appl. Phys.* **2018**, *51*, 115305. [CrossRef]
23. Cardoso, J.T.; Garcia-Giron, A.; Romano, J.M.; Huerta-Murillo, D.; Jagdheesh, R.; Walker, M.; Dimov, S.S.; Ocana, J.L. Influence of ambient conditions on the evolution of wettability properties of an IR-, ns-laser textured aluminium alloy. *RSC Adv.* **2017**, *7*, 39617–39627. [CrossRef]
24. Wang, H.; He, M.; Liu, H.; Guan, Y. One-step fabrication of robust superhydrophobic steel surfaces with mechanical durability, thermal stability, and anti-icing function. *ACS Appl. Mater. Interfaces* **2019**, *11*, 25586–25594. [CrossRef]
25. Volpe, A.; Gaudiuso, C.; Venere, L.D.; Licciulli, F.; Giordano, F.; Ancona, A.; Interateneo, D.; Amendola, V.G. Direct femtosecond laser fabrication of superhydrophobic aluminum alloy surfaces with anti-icing properties. *Coatings* **2020**, *10*, 587. [CrossRef]
26. Jagdheesh, R. Fabrication of a superhydrophobic Al_2O_3 surface using picosecond laser pulses. *Langmuir* **2014**, *30*, 12067–12073. [CrossRef]
27. Jagdheesh, R.; García-Ballesteros, J.J.; Ocaña, J.L. One-step fabrication of near superhydrophobic aluminum surface by nanosecond laser ablation. *Appl. Surf. Sci.* **2016**, *374*, 2–11. [CrossRef]
28. Milles, S.; Voisiat, B.; Nitschke, M.; Lasagni, A.F. Influence of roughness achieved by periodic structures on the wettability of aluminum using direct laser writing and direct laser interference patterning technology. *J. Mater. Process. Technol.* **2019**, *270*, 142–151. [CrossRef]
29. Bormashenko, E. Physics of solid-liquid interfaces: From the Young equation to the superhydrophobicity (review article). *Low Temp. Phys.* **2016**, *42*, 622–635. [CrossRef]
30. Chen, L.; Yang, G.; Wang, S. Air-grid surface patterning provided by superhydrophobic surfaces. *Small* **2012**, *8*, 962–965. [CrossRef] [PubMed]

31. Cheng, J.; Perrie, W.; Edwardson, S.P.; Fearon, E.; Dearden, G.; Watkins, K.G. Effects of laser operating parameters on metals micromachining with ultrafast lasers. *Appl. Surf. Sci.* **2009**, *256*, 1514–1520. [CrossRef]
32. ImageJ. Available online: https://imagej.nih.gov/ij/index.html (accessed on 10 March 2021).
33. Barani, J. Rain Drop Size and Speed of a Falling Rain Drop. Available online: https://www.baranidesign.com/faq-articles/2020/1/19/rain-drop-size-and-speed-of-a-falling-rain-drop#:~{}:text=Mostmeasurablerainfalldropsizes,thanastandardizedlaboratorydrop (accessed on 9 January 2021).
34. Callies, M.; Quéré, D. On water repellency. *Soft Matter* **2005**, *1*, 55–61. [CrossRef]
35. Van Den Brand, J.; Van Gils, S.; Beentjes, P.C.J.; Terryn, H.; De Wit, J.H.W. Ageing of aluminium oxide surfaces and their subsequent reactivity towards bonding with organic functional groups. *Appl. Surf. Sci.* **2004**, *235*, 465–474. [CrossRef]
36. Samaha, M.A.; Vahedi Tafreshi, H.; Gad-el-Hak, M. Sustainability of superhydrophobicity under pressure. *Phys. Fluids* **2012**, *24*, 112103. [CrossRef]
37. Shirtcliffe, N.J.; McHale, G.; Newton, M.I.; Perry, C.C.; Pyatt, F.B. Plastron properties of a superhydrophobic surface. *Appl. Phys. Lett.* **2006**, *89*, 10–12. [CrossRef]
38. Scarratt, L.R.J.; Steiner, U.; Neto, C. A review on the mechanical and thermodynamic robustness of superhydrophobic surfaces. *Adv. Colloid Interface Sci.* **2017**, *246*, 133–152. [CrossRef] [PubMed]
39. Li, Z.; Marlena, J.; Pranantyo, D.; Nguyen, B.L.; Yap, C.H. A porous superhydrophobic surface with active air plastron control for drag reduction and fluid impalement resistance. *J. Mater. Chem. A* **2019**, *7*, 16387–16396. [CrossRef]